

Article

# Sparsity-Inducing Super-Resolution Passive Radar Imaging with Illuminators of Opportunity

Shunsheng Zhang <sup>1,\*</sup>, Yongqiang Zhang <sup>1</sup>, Wen-Qin Wang <sup>1</sup>, Cheng Hu <sup>2</sup> and Tat Soon Yeo <sup>3</sup>

<sup>1</sup> Research Institute of Electronic Science and Technology, University of Electronic Science and Technology of China, Chengdu 611731, China; zhangyq116@163.com (Y.Z.); wqwang@uestc.edu.cn (W.Q.W.)

<sup>2</sup> Electronics and Information School, Beijing Institute of Technology, Beijing 100081, China; cchchb@163.com

<sup>3</sup> Department of Electrical and Computer Engineering, National University of Singapore, Singapore 117576, Singapore; eleyeots@nus.edu.sg

\* Correspondence: zhangss\_bit@163.com; Tel.: +86-28-6183-1163

Academic Editors: Daniele Riccio, Francesco Soldovieri, Raffaele Persico, Magaly Koch and Prasad S. Thenkabil

Received: 9 May 2016; Accepted: 19 October 2016; Published: 8 November 2016

**Abstract:** Multiple illuminators of opportunity (IOs) and a large rotation angle are often required for current passive radar imaging techniques. However, a large rotation angle demands a long observation time, which cannot be implemented for actual passive radar system. To overcome this disadvantage, this paper proposes a super-resolution passive radar imaging framework with a sparsity-inducing compressed sensing (CS) technique, which allows for fewer IOs and a smaller rotation angle. In the proposed imaging framework, the sparsity-based passive radar imaging is modeled mathematically, and the spatial frequencies and amplitudes of different scatterers on the target are recovered by the log-sum penalty function-based CS reconstruction algorithm. In doing so, a super-resolution passive radar imagery is obtained by the frequency searching approach. Simulation results not only validate that the proposed method outperforms existing super-resolution algorithms, such as ESPRIT and RELAX, especially in the cases with low signal-to-noise ratio (SNR) and limited number of measurements, but also have shown that our proposed method can perform robust reconstruction no matter if the target is on grid or not.

**Keywords:** sparsity-inducing; super-resolution; passive radar imaging; illuminator of opportunity (IO); compressed sensing (CS)

## 1. Introduction

Passive radar exploiting illuminator of opportunity (IO), such as frequency modulation (FM) station [1,2], television station [3], etc., has been shown to successfully detect and track targets [4–6]. While compared with active radar, passive radar has many advantages in low cost, low vulnerability to electronic jamming, counter low-flying target penetration and counter-stealth. Nevertheless, it is a challenge for existing passive radar techniques to achieve high-resolution imaging due to limited bandwidth of the opportunistic signals.

Conventional inverse synthetic aperture radar (ISAR) [7,8] usually transmits a large bandwidth signal to achieve fine range resolution. However, in passive radar imaging, most IOs just irradiate a narrow bandwidth signal in Ultra High Frequency (UHF) or Very High Frequency (VHF) bands. Furthermore, if the target rotation angle relative to the radar is also small, then the radar shall also have a very limited cross-range resolution. Even for a large rotation angle, more complicated target-motion compensation is often required due to non-uniform rotational motion and/or fluctuation of target reflection characteristics.

Several investigations have been performed for passive ISAR imaging [9–13]. In [9], a smoothed pseudo Wigner–Ville distribution (SPWVD) has been applied for passive ISAR cross-range processing to achieve wide-angle imaging. However, this algorithm requires a large number of illuminators to provide a large rotation angle and a large computation complexity induced by the time-frequency transform. In [10,11], an experiment to enhance the cross-range resolution of passive ISAR image using digital TV based passive bistatic radar (PBR) has been carried out. It is demonstrated that a moderate resolution can be expected for the polar format algorithm (PFA), but there is a tradeoff between the imaging swath and the resolution. In [12,13], a passive ISAR processing scheme is presented by exploiting the multichannel digital television broadcasting (DVB)-T signals, which is verified by the experimental results of ship and civilian aircraft imaging. Nevertheless, since the rotation angle is only several degrees, it is still difficult to obtain a meaningful passive ISAR image. Thus, a large rotation angle should be employed for the system. In general, a large rotation angle means a long observation time. However, when the target is maneuvering, the target may not be irradiated by the IO and passive radar simultaneously, which makes long-term data collection very difficult. Moreover, portions of the data may be missed due to uncooperative IO. To resolve these problems, effective algorithms should be developed for passive ISAR super-resolution imaging, particularly for the cases with a small rotation angle as well as with limited measurements.

In [14], an ESPRIT based super-resolution imaging algorithm based on external illuminators is proposed under the condition of small angular rotation, where ESPRIT [15] is used to estimate the spatial frequencies of different scatterers on the target. RELAX [16,17] can also estimate the amplitude and frequency of multi-component complex sinusoidal signals and has been successfully applied for super-resolution SAR imaging. Although the proposed scheme seems to work well for super-resolution passive radar imaging, we should be aware that both ESPRIT and RELAX are more or less sensitive to noise and modeling errors. In addition, applying ESPRIT or RELAX for passive radar imaging will require a considerable amount of measurements and, consequently, it is impractical for actual applications. A compressed sensing (CS) based algorithm was proposed in [18] to reconstruct passive ISAR images, but it is effective only when the multiple non-adjacent DVB-T channels are spectrally separated.

In this paper, we propose a super-resolution passive ISAR imaging framework based on CS for the case with two illuminators and a small rotation angle. In this framework, the passive radar imaging is recast as a reconstruction problem of sparse signal with unknown amplitude and frequency. Next, the log-sum penalty function-based CS algorithm is employed to recover the amplitude and frequency parameters of strong scatterers. Simulated results demonstrate the superiority of the proposed method over other existing super-resolution algorithms such as ESPRIT and RELAX under the condition of low SNR and limited measurements.

The remaining sections are organized as follows. In Section 2, the parametric passive radar imaging model is established. Section 3 presents the CS-based algorithm for super-resolution passive radar image formation. In Section 4, we compare the performance of the proposed algorithm and other super-resolution algorithms with simulated data. Finally, conclusions are drawn in Section 5.

## 2. Parametric Passive Radar Imaging Model

Consider a two-dimensional imaging model as shown in Figure 1. The reference point  $O$  is taken at the target center,  $T(r_i, \theta_i)$  and  $R(r_0, \theta_0)$  denote the  $i$ -th ( $i = 1, 2$ ) illuminator and receiver coordinates, respectively;  $P_k(r_k, \varphi_k)$  denotes the  $k$ -th ( $k = 1, 2, \dots, K$ ) scatterer's coordinates on the target, and the distances from the  $k$ -th scatterer to the  $i$ -th illuminator and receiver are denoted by  $R_i^k$  and  $R_0^k$ , respectively.

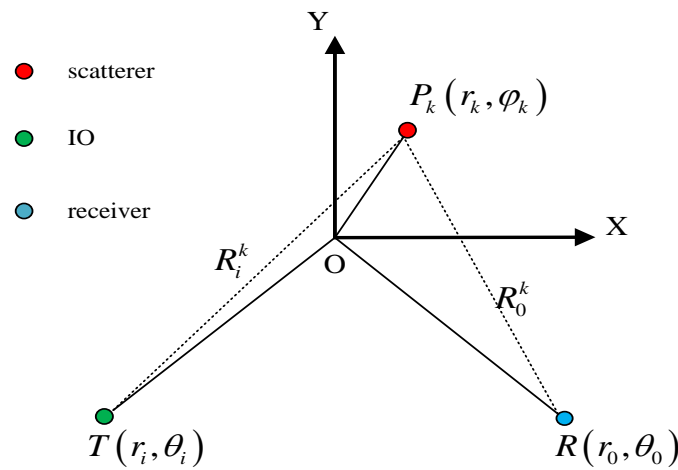


Figure 1. Passive radar imaging model.

Suppose the  $i$ -th illuminator transmits a monochromatic continuous signal [19–21]

$$s_i(t) = \exp(j2\pi f_i t), \tag{1}$$

where  $t$  is the fast time and  $f_i$  is the carrier frequency. The received signal reflected from the  $k$ -th scatterer is

$$s_i(t, \tau) = A_k \exp[j2\pi f_i (t - \tau)], \tag{2}$$

where  $A_k$  is the reflectivity of the  $k$ -th scatterer, and  $\tau$  is the signal propagation time determined by

$$\tau = \frac{R_i^k + R_0^k}{c}, \tag{3}$$

with  $c$  being the speed of light. In the far-field condition, since  $R_i^k \gg r_k$  and  $R_0^k \gg r_k$ , we can use the following approximations

$$R_i^k \approx r_i - r_k \cos(\varphi_k - \theta_i), \tag{4}$$

$$R_0^k \approx r_0 - r_k \cos(\varphi_k - \theta_0), \tag{5}$$

Then, Equation (2) can be rewritten as

$$s(t) = A_k \exp \left[ j2\pi \left( f_i t - \frac{r_i + r_0}{\lambda_i} \right) \right] \times \exp \left\{ j \frac{2\pi}{\lambda_i} [r_k \cos(\varphi_k - \theta_i) + r_k \cos(\varphi_k - \theta_0)] \right\}, \tag{6}$$

with  $\lambda_i = c/f_i$  being the wavelength. Assuming that the referenced signal is

$$s_{ref}(t) = \exp \left[ j2\pi \left( f_i t - \frac{r_i + r_0}{\lambda_i} \right) \right], \tag{7}$$

the instantaneous complex envelope of the returned signal after demodulation and translational motion compensation can be represented by

$$s = A_k \exp \left\{ j \frac{2\pi}{\lambda_i} [r_k \cos(\varphi_k - \theta_i) + r_k \cos(\varphi_k - \theta_0)] \right\}. \tag{8}$$

Note that stationary illuminators and receiver and moving target are assumed. In this case, the rotation velocity can be estimated by the method presented in [19], wherein both a short observation

time and corresponding small rotation angle that can be regarded as uniform rotation are assumed. In this paper, we suppose the target moves with a rotation angle  $\Theta$  during the observation time and define the instantaneous rotation angle as  $\varphi_{\Theta} \in [\varphi_k - \Theta, \varphi_k]$ . Thus, Equation (8) can be rewritten as

$$s(\varphi_{\Theta}) = A_k \exp \left\{ j \frac{2\pi}{\lambda_i} [r_k \cos(\varphi_{\Theta} - \theta_i) + r_k \cos(\varphi_{\Theta} - \theta_0)] \right\}. \quad (9)$$

Let  $(\theta_0 - \theta_i) / 2 = \beta$ ,  $(\theta_0 + \theta_i) / 2 = \alpha$ ,  $\cos(\beta) / \lambda = \zeta$  and  $\varphi_{\Theta} = \varphi_k - \Theta$ , (9) be reformulated through the trigonometrical transform into

$$s(\Theta) = A_k \exp \{ j4\pi\zeta r_k [\cos(\varphi_k - \alpha) \cos \Theta - \sin(\varphi_k - \alpha) \sin \Theta] \}. \quad (10)$$

For such a small rotation angle, we have

$$\begin{aligned} \cos \Theta &\approx 1, \\ \sin \Theta &\approx \Theta. \end{aligned} \quad (11)$$

Substituting Equation (11) into Equation (10) yields

$$s(\Theta) = A_k \exp [j4\pi\zeta r_k \cos(\varphi_k - \alpha)] \times \exp [-j4\pi\zeta r_k \sin(\varphi_k - \alpha) \Theta]. \quad (12)$$

Let  $h(k) = A_k \exp [j4\pi\zeta r_k \cos(\varphi_k - \alpha)]$  and  $\omega_k = -4\pi\zeta r_k \sin(\varphi_k - \alpha)$ , (12) can be rewritten as

$$s(\Theta) = h(k) \exp(j\Theta\omega_k). \quad (13)$$

Suppose the target consists of  $K$  scatterers, the received signal can then be represented by

$$s(\Theta) = \sum_{k=0}^{K-1} h(k) \exp(j\Theta\omega_k), \quad (14)$$

where  $h(k)$  and  $\omega_k$  are the reflected amplitude and spatial frequency of the  $k$ -th scatterer, respectively. Equation (14) implies that the returned signal can be parameterized as a summation of  $K$  sinusoids with unknown amplitudes and frequencies. Moreover, in the passive radar imagery, strong scatterers often only take up a fraction of the two-dimensional imaging scene. Therefore, passive radar imaging can be regarded as a sparse reconstruction problem, and, thus, we propose the following passive radar super-resolution imaging algorithm with a CS technique.

### 3. Super-Resolution Imaging for Passive Radar

The ESPRIT algorithm for passive radar imaging has been investigated in [14], which employs the rotation invariance technique and eigenvalue decomposition to estimate the amplitude and spatial frequency of each scatterer. In this section, two super-resolution algorithms including RELAX and CS are presented in detail.

After discretization, Equation (14) can be rewritten as

$$s(m) = \sum_{k=0}^{K-1} h(k) \exp[jm\Delta\Theta \cdot \omega_k], \quad (15)$$

where  $\Theta = m\Delta\Theta$ ,  $m = 0, 1, \dots, M-1$ , with  $m$  being the sampling number. Then, Equation (15) can be reformulated as the vector-matrix form

$$\mathbf{s} = \mathbf{Q}\mathbf{h}, \quad (16)$$

where  $\mathbf{s} = [s(0), s(1), \dots, s(M-1)]^T$ ,  $\mathbf{Q} = [f(\omega_0), f(\omega_1), \dots, f(\omega_{K-1})]$ ,  $f(\omega_k) = [1, e^{j\Delta\Theta\omega_k}, e^{j2\Delta\Theta\omega_k}, \dots, e^{j(M-1)\Delta\Theta\omega_k}]^T$ ,  $(k = 0, 1, \dots, K-1)$ ,  $\mathbf{h} = [h(0), h(1), \dots, h(K-1)]^T$ , with  $[\cdot]^T$  being the transpose operator.

### 3.1. RELAX-Based Passive Radar Imaging

RELAX, which relaxes the hypothesis of the additive noise and system errors, is an effective spectrum estimation algorithm. By adopting an iterative procedure, the spatial frequencies of the scatterers can be estimated by the nonlinear least square (NLS) method. When the RELAX algorithm is employed, Equation (16) should be recast as:

$$\{h', \omega'\} = \arg \min_{h, \omega} \|s - \mathbf{Q}h\|_2^2, \quad (17)$$

where  $h'$  and  $\omega'$  are the estimates of  $h$  and  $\omega$ , respectively; and  $\|\cdot\|_2$  denotes the  $\ell_2$  norm. Let

$$s_k = s - \sum_{i=0, i \neq k}^{K-1} h'(i) f(\omega'_i), \quad (18)$$

where  $\{h'(i), \omega'_i\}$  ( $i = 0, 1, \dots, K-1, i \neq k$ ) are assumed to be given. Then, the minimization of Equation (17) is equivalent to

$$\{h'(k), \omega'_k\} = \arg \min_{h(k), \omega_k} \|s_k - h(k) f(\omega_k)\|_2^2. \quad (19)$$

The NLS estimates of  $h'(k)$  and  $\omega'_k$  are given by [16], respectively:

$$h'(k) = \frac{f^H(\omega'_k) s_k}{M}, \quad (20)$$

$$\omega'_k = \arg \max_{\omega_k} \|f^H(\omega_k) s_k\|_2^2. \quad (21)$$

It should be noted that  $\omega'_k$  is the dominant peak position of  $\|f^H(\omega_k) s_k\|_2^2$ , which can be efficiently obtained by fast Fourier transform (FFT) for the data sequence  $s_k$  padded with zeros. According to [22], the locally optimal solution of  $\{h'(i), \omega'_i\}$  obtained by the NLS estimate is globally optimal. That is, we can obtain two independent sets  $\{h', \omega'\}$  estimated from the two external illuminators. Subsequently, a passive ISAR image can then be attained with these two estimated sets  $\{h', \omega'\}$ .

### 3.2. CS-Based Passive Radar Super-Resolution Imaging

It is widely recognized that in the CS framework, the optimal reconstruction of an unknown sparse signal can be achieved from limited noisy measurements by solving a sparsity-constrained optimization problem [23]. The CS framework has been successfully applied in conventional ISAR and bistatic ISAR imaging [24–27]. In this paper, we use such a CS technique to accomplish super-resolution passive radar imaging with fewer television illuminators and a smaller rotation angle.

Taking additive noise into account, Equation (16) can then be rewritten as

$$s = \Phi h + \sigma, \quad (22)$$

where  $h = [h(0), h(1), \dots, h(N-1)]^T$ ,  $\sigma$  is the measured noise,  $\Phi$  is the dictionary matrix, and the  $(k, m)$  element of  $\Phi$  is defined as:

$$\phi_k(m) = \exp(-j\omega_k \cdot m\Delta\Theta). \quad (23)$$

Note that the dictionary  $\Phi$  is characterized by unknown parameters  $\{\omega_k\}$ , which should be estimated together with the unknown complex amplitude  $\{h_k\}$ . Estimating  $\{\omega_k\}$  and  $\{h_k\}$  can then be formulated as a sparse recovery problem:

$$\begin{aligned} \min_{\mathbf{h}} \quad & \|\mathbf{h}\|_1, \\ \text{s.t.} \quad & \|\mathbf{s} - \Phi\mathbf{h}\|_2 < \delta, \end{aligned} \tag{24}$$

where  $\|\cdot\|_1$  denotes the  $\ell_1$  norm,  $\delta$  is the noise level, and  $\Phi \in \mathbb{C}^{M \times N}$  ( $M \ll N$ ,  $N$  is the length of the recovered signal) is an over-complete dictionary. Accurate reconstruction of the sparse signal can be achieved through existing recovery algorithms, such as orthogonal matching pursuit (OMP) [28] and basis pursuit (BP) [29].

In this paper, we use a log-sum sparsity-encouraging function for the sparse reconstruction. The log-sum penalty function has been extensively applied for sparse signal recovery [30–32], and its superiority over the conventional  $\ell_1$ -type algorithm has been widely verified. In doing so, Equation (24) can be recast as

$$\begin{aligned} \min_{\mathbf{h}} \quad & L(\mathbf{h}) = \sum_{i=1}^N \log(|h_i|^2 + \epsilon'), \\ \text{s.t.} \quad & \|\mathbf{s} - \Phi\mathbf{h}\|_2 < \delta, \end{aligned} \tag{25}$$

where  $h_i$  denotes the  $i$ -th component of the vector  $\mathbf{h}$ , and  $\epsilon' > 0$  is a positive parameter to ensure that the function is well-defined. Thus, the  $\{\omega_k\}$  and  $\{h_k\}$  can be estimated by the algorithm proposed in [33].

Once the amplitude and spatial frequency of each scatterer are obtained, the target position can be determined by searching the vector  $\omega' = \{\omega_k\}_{k=1}^K$ . Here, it should be pointed out that the passive radar image achieved in this paper is a two-dimensional image. Thus, at least two illuminators are needed. Thus, the scatterers' position estimation problem can be further formulated as

$$\{\mathbf{r}', \boldsymbol{\varphi}'\} = \arg \min_{\mathbf{r}, \boldsymbol{\varphi}} \|\omega_{ref} - \omega'\|_{2'} \tag{26}$$

where  $\{\mathbf{r}', \boldsymbol{\varphi}'\}$  are the estimates of  $\{r_i, \varphi_i\}_{i=1}^K$ , and  $\omega_{ref}$  is the referenced spatial frequency. The position information of different scatterers can then be obtained by solving Equation (26).

In summary, the flowchart of the proposed CS-based method for passive radar imaging is shown in Figure 2. After searching for positions using two sets of  $\omega'$ , and adding the scattering amplitude information in the reconstructed vector  $\mathbf{h}'$ , we can obtain the passive radar image of the target.

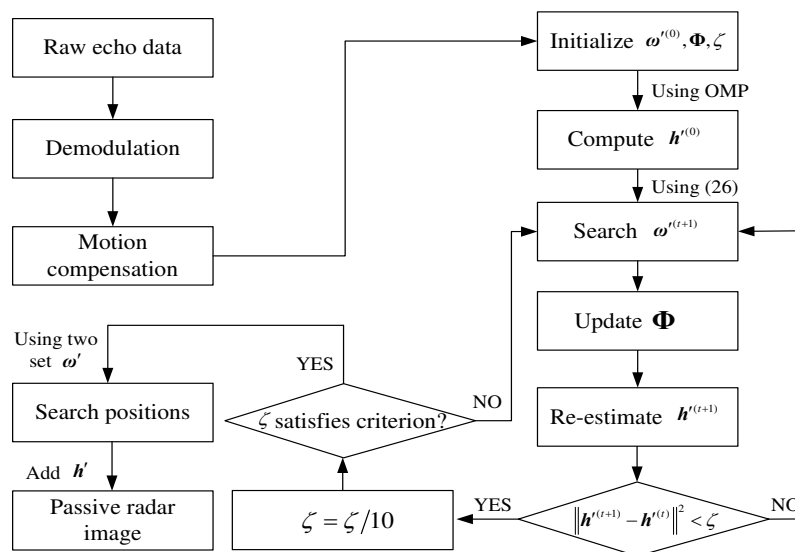


**Figure 2.** Flowchart of the proposed compressed sensing (CS)-based method for passive radar imaging.

### 3.3. Further Discussions

#### 3.3.1. Influence of Noise

It should be emphasized that the use of the ESPRIT algorithm for super-resolution passive radar imaging requires a high SNR ( $\text{SNR} \geq 30$  dB). Otherwise, it will have a large reconstruction error. In contrast, the RELAX and CS methods achieve good recovery performance even in low SNR cases.

In addition, the estimation of the noise level given in Equation (25) is still an open problem in sparse signal recovery. If  $\delta$  is too large, a part of the signal component cannot be recovered. On the other hand, if  $\delta$  is too small, some noise components may be treated as signals. In this paper, we estimate the noise level  $\delta$  using the energy-based method presented in [34].

#### 3.3.2. Influence of Measurements

In CS-based passive radar imaging, accurate frequency estimation can be obtained only when a large  $M$  is employed. In our algorithm, we only require that  $M \geq O(K \log(N/K))$  for Equation (25). In contrast, our investigations (detailed in Section 4) demonstrate that ESPRIT and RELAX algorithms cannot yield accurate frequency estimation for such a small  $M$ . This implies that our proposed CS algorithm can achieve better frequency estimation performance than the ESPRIT and RELAX algorithms when limited measurements are available.

#### 3.3.3. Why CS Performs Better Than ESPRIT and RELAX

While both the ESPRIT and RELAX algorithms have been shown to be able to perform super-resolution imaging through spectra estimation; however, their reconstruction performance are restricted by the length of the measured data. For limited observation data, the passive radar imaging results obtained by the ESPRIT and RELAX algorithms will be very poor, which have been validated in Section 4.5. On the contrary, the proposed CS method can reconstruct a high-dimensional signal from low-dimensional observation data. This reason is that an unknown sparse signal may be accurately recovered from a limited number of measurements by solving a sparsity-driven optimization problem. In other words, the CS-based method is not sensitive to the data limitation. Therefore, CS can achieve better reconstruction performance than the ESPRIT and RELAX algorithms in super-resolution passive radar imaging.

## 4. Simulation and Analysis

In this section, we use simulation data to evaluate the performance of the proposed method, and compare it with the ESPRIT and RELAX algorithms under different SNRs and limited measurement conditions.

Suppose the illuminator of opportunity A, represented by IO(A), locates at (35 km,  $80^\circ$ ) and operates at the carrier frequency of 200 MHz, while the illuminator of opportunity B, denoted by IO(B), locates at (30 km,  $20^\circ$ ) and works at 280 MHz. The receiver is located at (20 km,  $0^\circ$ ). Additionally, the rotation angle  $\Theta$  is assumed to be  $4^\circ$  during the observation time.

### 4.1. Frequency Estimation of Scatterers Applying CS

The noise corrupted data with  $\text{SNR} = 20$  dB is generated by adding white Gaussian noise into the simulated passive radar echo. Then, the proposed CS method is applied to estimate the amplitudes and spatial frequencies of six scatterers  $((0,0), (3,0), (3,9\pi/16), (3,-9\pi/16), (3,15\pi/16), (3,-15\pi/16))$  on the target. To provide a quantitative evaluation for estimation performance, the relative mean square error (MSE) is defined by

$$\text{MSE} = \frac{\|\omega' - \omega\|_2}{\|\omega\|_2}, \quad (27)$$

where  $\omega'$ ,  $\omega$  represent the spatial frequency vector and its estimation of the scatterers, respectively.

Tables 1 and 2 give the MSE of the estimated spatial frequency from IO(A) and IO(B) using the proposed CS method, respectively, where the MSEs are calculated according to Equation (27). It can be observed that the estimated frequencies coincide with the theoretical values. This indicates that the proposed CS method can estimate the frequency parameter with high accuracy.

**Table 1.** Estimated spatial frequency and its mean-square-error (MSE) from illuminator of opportunity (IO) (A) using the proposed compressed sensing (CS) method.

| Scatterers              | 1      | 2       | 3       | 4        | 5      | 6       |
|-------------------------|--------|---------|---------|----------|--------|---------|
| Theoretical value (MHz) | 0      | −4.2980 | 24.7450 | −23.0681 | 8.9707 | −0.5399 |
| Estimated value (MHz)   | 0.1050 | −4.2910 | 24.7400 | −23.0770 | 8.9580 | −0.5340 |
| MSE (%)                 |        |         | 0.12    |          |        |         |

**Table 2.** Estimated spatial frequency and its MSE from IO(B) using the proposed CS method.

| Scatterers              | 1       | 2        | 3       | 4        | 5       | 6       |
|-------------------------|---------|----------|---------|----------|---------|---------|
| Theoretical value (MHz) | 0       | −17.3256 | 23.6312 | −16.8711 | 21.0209 | 12.9645 |
| Estimated value (MHz)   | −0.0110 | −17.1390 | 23.4770 | −16.7030 | 21.0270 | 12.9720 |
| MSE (%)                 |         |          | 0.14    |          |         |         |

#### 4.2. Position Estimation Using the Proposed Method

In this section, we demonstrate that the scatterer's position can be obtained through two frequency vectors. The simulation parameters are the same as Section 4.1. We first use one set  $\omega'$  to search for the position of the scatterer (3, 0), which is shown in Figure 3a. Obviously, the scatterer (3, 0) cannot be distinguished in the polar plane. In Figure 3b, the red point corresponds to the position of the scatterer (3, 0) estimated by using two frequency sets. Likewise, we use two frequency sets to estimate the position of six scatterers via (26), as shown in Figure 4. It is clear that the coordinates of all scatterers are correctly estimated.

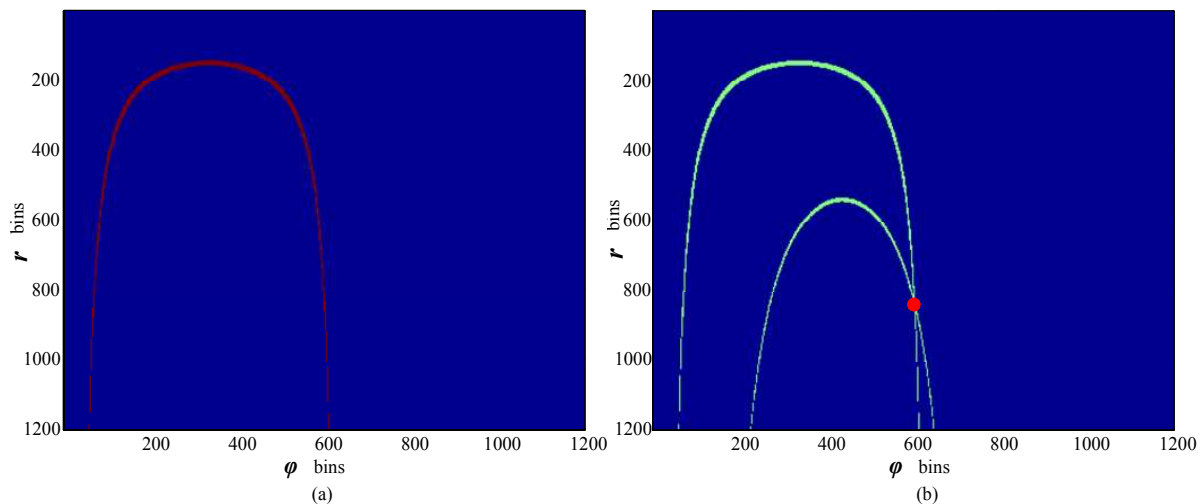


**Figure 3.** Position estimation of the scatterer located at (3, 0): (a) using single frequency set; and (b) using two frequency sets.

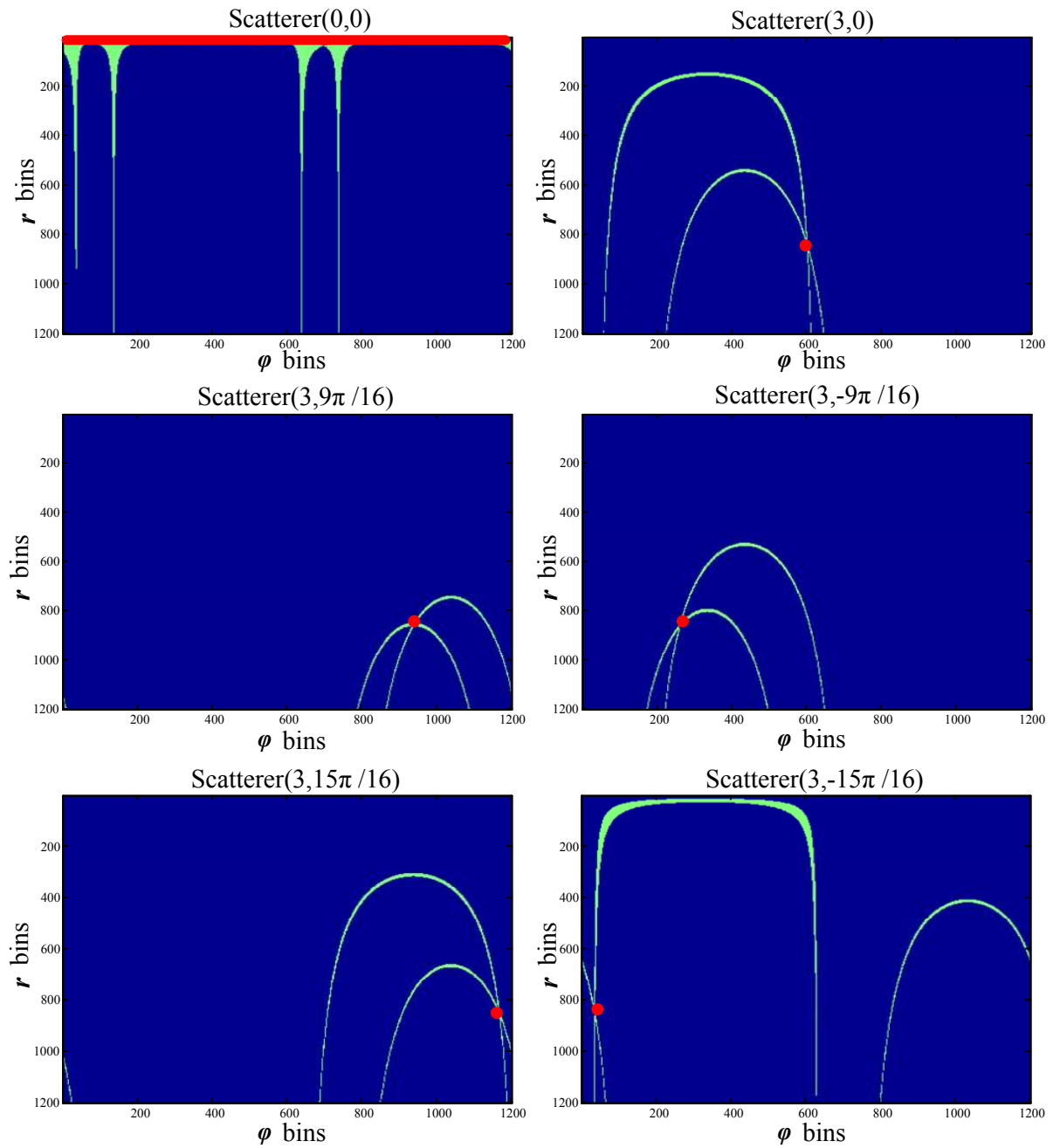
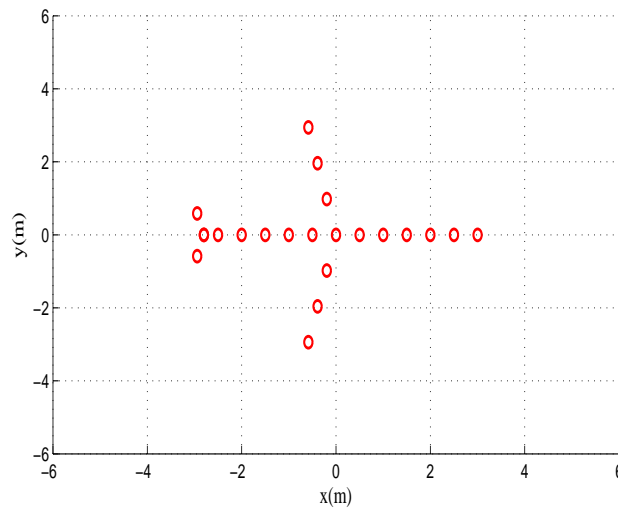


Figure 4. Position estimation of six scatterers using two frequency sets.

### 4.3. Resolution Comparison

In order to investigate the imaging resolution, an experiment of resolution comparison is carried out. The simulation parameters are the same as Section 4.1, and the scattering model of an extended target in the 2D plane is illustrated in Figure 5.



**Figure 5.** Scattering model of an extended target in the 2D plane.

Figure 6a corresponds to the reconstructed passive radar image obtained through the polar format algorithm (PFA) [10], and Figure 6b shows the passive radar imaging result reconstructed by the proposed method. We note that the passive radar image produced by our proposed method has better reconstruction performance than that of the PFA algorithm. Moreover, the proposed method can obtain higher resolution in the  $x$ - and  $y$ -direction than the PFA algorithm. This implies that our proposed method can achieve super-resolution. In addition, we find that when these scatterers are not on the grid, the proposed CS method can still obtain the focused image.

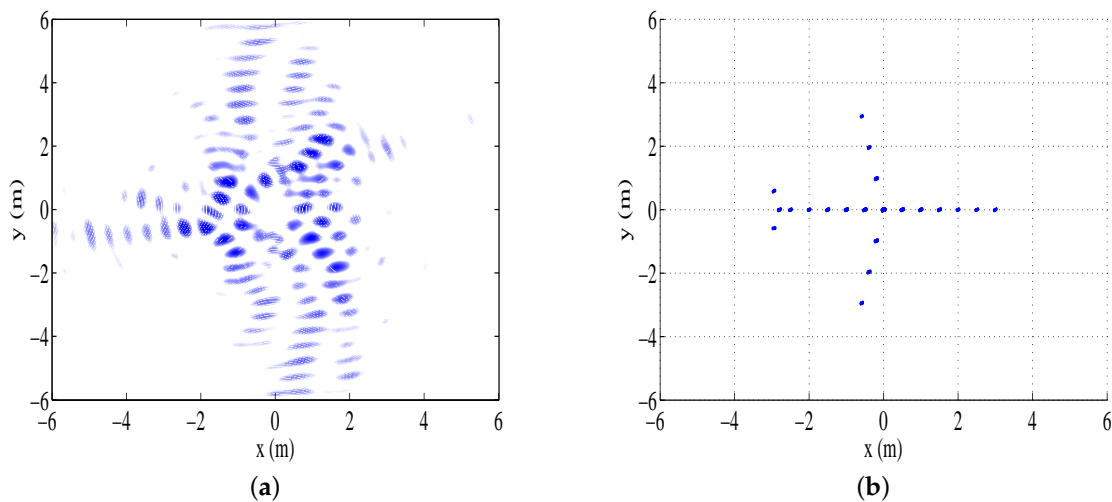


**Figure 6.** Passive radar images obtained by using different methods: (a) reconstructed image with the polar format algorithm (PFA); and (b) reconstructed image with the proposed method.

#### 4.4. Imaging Performance versus SNR

In this simulation, we examine the impacts of SNR on the passive radar imaging performance. We add different complex noise with Gaussian distribution into the simulated passive radar echoes with a SNR of 5, 10 and 20 dB, respectively. Similarly, the MSE of the estimated scatterers' position is used to evaluate the reconstruction performance.

Figure 7 compares the performance of the ESPRIT, RELAX and proposed CS algorithms in the passive radar imaging under different SNRs. The first, second and third row represent passive radar image obtained by the ESPRIT, RELAX and proposed CS algorithm, respectively. Note that the RELAX and proposed CS algorithms can provide position estimation with better accuracy than the ESPRIT algorithm under different SNR conditions. It should be emphasized that, among these three super-resolution algorithms, the estimation precision of the proposed CS algorithm is the highest under the same SNR condition.

It can be concluded from the MSE results given in Table 3 that, with decreasing SNR, the MSE of the estimated position obtained by the ESPRIT algorithm degrades rapidly. This implies that the noise level has a great effect on its estimation performance. However, the MSEs obtained by the RELAX and proposed CS algorithms are acceptable under different SNRs. Moreover, the proposed CS algorithm outperforms the RELAX algorithm in the sense of estimation accuracy. Even if the SNR is lower than 0 dB, for example,  $-10$  dB, the performance of the proposed CS-based passive radar imaging framework degrades slightly. Therefore, we can conclude that the proposed CS algorithm is suitable for super-resolution passive radar imaging, especially in low SNR situations.

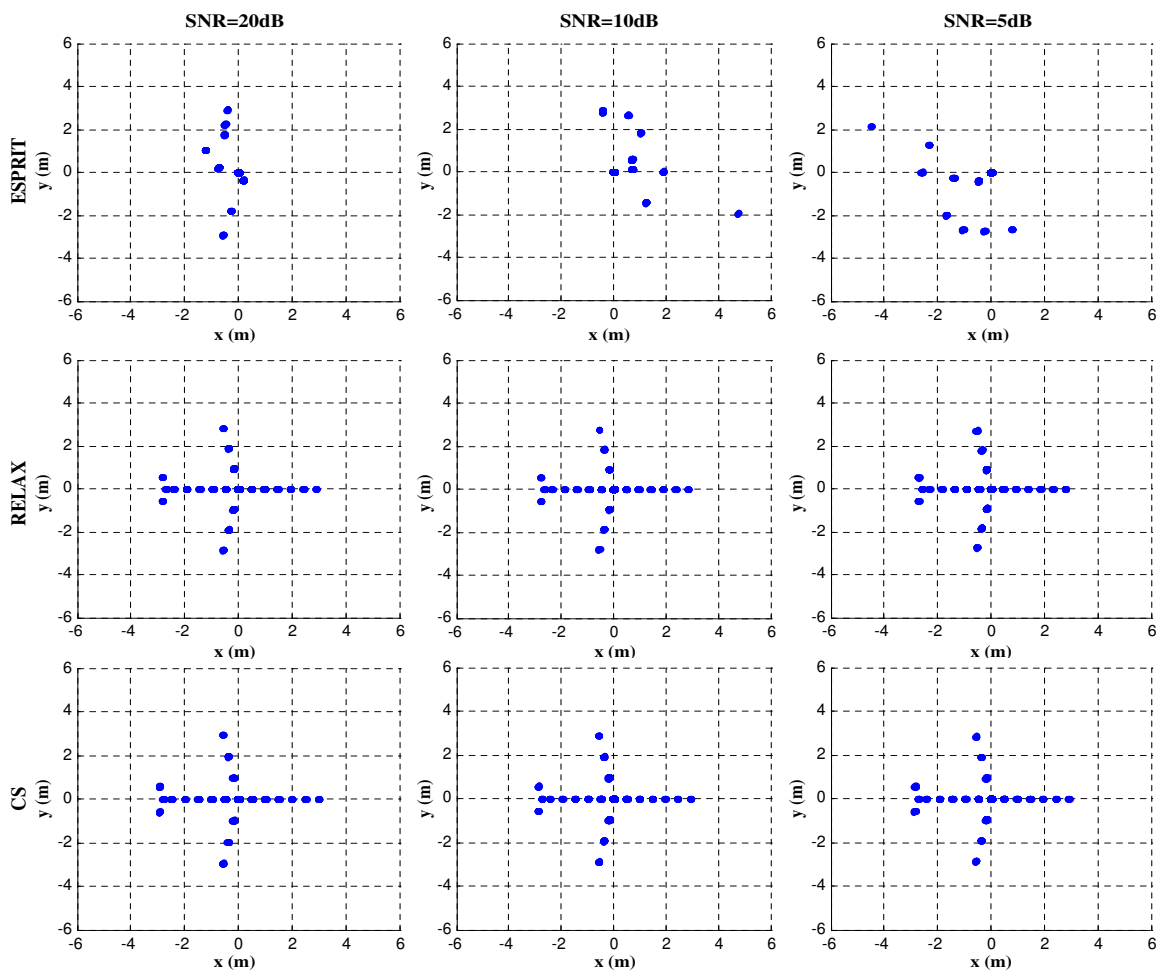


**Figure 7.** Passive inverse synthetic aperture radar (ISAR) imaging results with different reconstruction methods under different signal-to-noise ratios (SNRs).

**Table 3.** MSEs of the estimated position using the ESPRIT, RELAX and proposed CS algorithms under different signal-to-noise ratios (SNRs).

| Super-Resolution Algorithm |        |        |             |
|----------------------------|--------|--------|-------------|
| SNR (dB)                   | ESPRIT | RELAX  | Proposed CS |
| 20                         | 0.3560 | 0.0095 | 0.0023      |
| 10                         | 0.4045 | 0.0154 | 0.0025      |
| 5                          | 0.4608 | 0.0279 | 0.0029      |

4.5. Imaging Performance versus Measurements

In this experiment, we compare the reconstruction performance of different super-resolution algorithms in different amount of available measurement data. The used measurement data are 50%, 25% and 12.5% of the passive radar echo data, respectively, which can be obtained through two, four and eight times uniform decimation. Suppose the input SNR is 10 dB. The comparative imaging results are shown in Figure 8. The first, second and third rows represent super-resolution passive radar image obtained by the ESPRIT, RELAX and proposed CS algorithms, respectively. It is noticeable that the proposed CS algorithm can achieve more accurate reconstruction than both the ESPRIT and RELAX algorithms, even if the measured data is only 12.5% of the passive radar echo data.

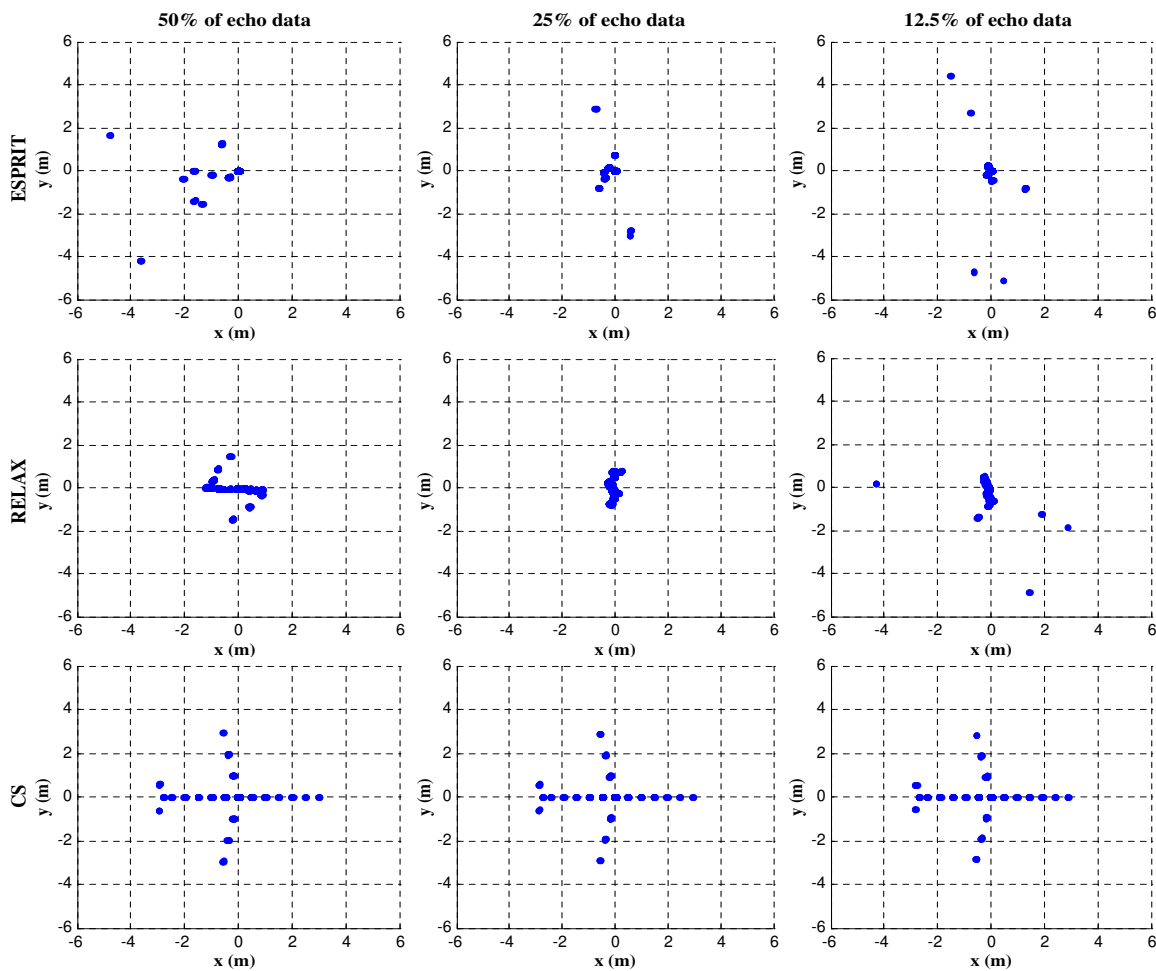


**Figure 8.** Passive ISAR imaging results with different reconstruction methods under different measurements.

It can be noticed from the estimation MSEs given in Table 4 that the ESPRIT and RELAX algorithms are heavily influenced by the amount of measurement data. In contrast, the proposed CS algorithm achieves satisfactory MSE even with very limited amount of measurement data. This validates again that the proposed CS algorithm is very effective for super-resolution radar imaging in limited measurement cases. However, when the used measured data is less than 1/16 of the original passive radar echo data, the imaging performance of the proposed framework will be seriously deteriorated, and corresponding MSE of the proposed CS algorithm is about 0.1625.

**Table 4.** MSEs of the estimated position using the ESPRIT, RELAX and proposed CS algorithms under different measurements.

| Measurements       | Super-Resolution Algorithm |        |             |
|--------------------|----------------------------|--------|-------------|
|                    | ESPRIT                     | RELAX  | Proposed CS |
| 50% of echo data   | 0.4028                     | 0.1854 | 0.0017      |
| 25% of echo data   | 0.5223                     | 0.2931 | 0.0075      |
| 12.5% of echo data | 0.9830                     | 0.7796 | 0.0143      |

## 5. Conclusions

This paper proposed a super-resolution passive radar imaging algorithm based on CS using a log-sum penalty function. After establishing the sparse signal model of passive radar imaging, we apply the CS technique to extract the spatial frequencies and scattering amplitudes of different scatterers. Next, the super-resolution passive radar imagery is reconstructed by searching the coordinates of each scatterer. Simulated data experiments have been provided to demonstrate that the proposed CS method outperforms other existing super-resolution algorithms such as ESPRIT and RELAX algorithms under both low SNR and limited measurement data. We have also shown that the proposed CS method allows for only two television illuminators and a small rotation angle to achieve super-resolution passive radar imaging. Furthermore, the proposed CS method can provide a new prospect to solve the off-grid problem.

**Acknowledgments:** This work was supported by the National Natural Science Foundation of China under grant 61671122 and 61571081.

**Author Contributions:** Shunsheng Zhang, Yongqiang Zhang, Cheng Hu and Wen-Qin Wang designed the research, performed data analysis; Shunsheng Zhang and Tat Soon Yeo contributed ideas and discussion.

**Conflicts of Interest:** The authors declare no conflict of interest.

## References

1. Howland, P.E.; Maksimiuk, D.; Reitsma, G. FM radio based bistatic radar. *IEE P-Radar Sonar Navig.* **2005**, *152*, 107–115.
2. Dilallo, A.; Farina, A.; Fulcoli, R.; Genovesi, P.; Lalli, R.; Mancinelli, R. Design, development and test on real data of an FM based prototypical passive radar. In Proceedings of the IEEE Radar Conference, Rome, Italy, 26–30 May 2008; pp. 1–6.
3. Glende, M.; Heckenbach, J.; Kuschel, H.; Muller, S.; Schell, J.; Schumacher, C. Experimental passive radar system using digital illuminators (DAB/DVB-T). In Proceedings of the International Radar Symposium, Cologne, Germany, 5–7 September 2007.
4. Raout, J. Sea target detection using passive DVB-T based radar. In Proceedings of the 2008 International Conference on Radar, Adelaide, Australia, 2–5 September 2008; pp. 695–700.
5. Sun, H.; Tan, D. K.; Lu, Y.; Lesturgie, M. Applications of passive surveillance radar system using cell phone base station illuminators. *IEEE Aerosp. Electron. Syst. Mag.* **2010**, *25*, 10–18.
6. Howland, P.E. Target tracking using television-based bistatic radar. *IEE P-Radar Sonar Navig.* **1999**, *146*, 166–174.

7. Wang, Y.; Jiang, Y. ISAR imaging of non-uniform rotating target via range instantaneous Doppler derivatives algorithm. *IEEE J. Sel. Top. Appl. Earth Observ. Remote Sens.* **2014**, *7*, 167–176.
8. Zhang, S.; Sun, S.; Zhang, W.; Zong, Z.; Yeo, T.S. High-resolution bistatic ISAR image formation for high-speed and complex-motion targets. *IEEE J. Sel. Top. Appl. Earth Observ. Remote Sens.* **2015**, *8*, 3520–3531.
9. Wu, Y.; Munson, D.C. Wide-angle ISAR passive imaging using soothed pseudo Wigner-Ville distribution. In Proceedings of the 2001 IEEE Radar Conference, Atlanta, GA, USA, 1–3 May 2001; pp. 363–368.
10. Suwa, K.; Nakamura, S.; Morita, S.; Wakayama, T.; Maniwa, H.; Oshima, T.; Maekawa, R.; Matsuda, S.; Tachihara, T. ISAR imaging of an aircraft target using ISDB-T digital TV based passive bistatic radar. In Proceedings of the IEEE International Geoscience and Remote Sensing Symposium, Honolulu, HI, USA, 25–30 July 2010; pp. 4103–4105.
11. Nakamura, S.; Suwa, K.; Morita, S.; Yamamoto, K.; Wakayama, T.; Oshima, T.; Maekawa, R.; Matsuda, S. An experimental study of enhancement of the cross-range resolution of ISAR imaging using ISDB-T digital TV based bistatic radar. In Proceedings of the IEEE International Geoscience and Remote Sensing Symposium, Vancouver, BC, Canada, 24–29 July 2011; pp. 2837–2840.
12. Olivadese, D.; Giusti, E.; Petri, D.; Martorella, M.; Capria, A.; Berizzi, F.; Soletti, R. Passive ISAR imaging of ships by using DVB-T signals. In Proceedings of the IET International Conference on Radar Systems, Glasgow, UK, 22–25 October 2012; pp. 287–290.
13. Olivadese, D.; Giusti, E.; Petri, D.; Martorella, M.; Capria, A.; Berizzi, F. Passive ISAR imaging with DVB-T Signals. *IEEE Trans. Geosci. Remote Sens.* **2013**, *51*, 4508–4517.
14. Li, Y.; Liu, J. ESPRIT super-resolution imaging algorithm based on external illuminators. In Proceedings of the 1st Asian and Pacific Conference on Synthetic Aperture Radar, Huanshan, China, 5–9 November 2007; pp. 232–235.
15. Roy, R.; Kailath, T. ESPRIT—Estimation of signal parameters via rotational invariance techniques. *IEEE Trans. Acoust. Speech Signal Process.* **1999**, *37*, 984–995.
16. Li, J.; Stoica, P. Efficient mixed-spectrum estimation with applications to target feature extraction. *IEEE Trans. Signal Process.* **1996**, *44*, 281–295.
17. Bi, Z.; Li, J.; Liu, Z. Super resolution SAR imaging via parametric spectral estimation methods. *IEEE Trans. Aerosp. Electron. Syst.* **1999**, *35*, 267–281.
18. Qiu, W.; Giusti, E.; Martorella, M.; Berizzi, F.; Zhao, H.; Fu, Q. Compressive sensing for passive ISAR with DVB-T signal. In Proceedings of the International Radar Symposium, Dresden, Germany, 19–21 June 2013; pp. 113–118.
19. Wang, S.; Tang, Y.; Liu, C.; Wang, T.; Chen, W. Sparse passive radar imaging based on FM stations using the U-ESPRIT for moving target. In Proceedings of the IET International Radar Conference, Xi'an, China, 14–16 April 2013; pp. 1–6.
20. Yarman, C. E.; Wang, L.; Yazici, B. Passive synthetic aperture radar imaging with single-frequency sources of opportunity. In Proceedings of the IEEE Radar Conference, Washington, DC, USA, 10–14 May 2010; pp. 949–954.
21. Mason, E.; Son, I.Y.; Yazici, B. Passive synthetic aperture radar imaging using low-rank matrix recovery methods. *IEEE J. Sel. Topics Signal Process.* **2015**, *9*, 1570–1582.
22. Jennrich, R.I. Asymptotic properties of nonlinear least squares estimators. *Ann. Appl. Stat.* **1969**, *40*, 633–643.
23. Candes, E.; Romberg, J.; Tao, T. Robust uncertainly principles: Exact signal reconstruction from highly incomplete frequency information. *IEEE Trans. Inf. Theory* **2006**, *52*, 489–509.
24. Zhang, S.; Xiao, B.; Zong, Z. Improved compressed sensing for high-resolution ISAR image reconstruction. *Chin. Sci. Bull.* **2014**, *59*, 2918–2926.
25. Rao, W.; Li, G.; Wang, X.; Xia, X.G. Adaptive sparse recovery by parametric  $l_1$  weighted minimization for ISAR imaging of uniformly rotating targets. *IEEE J. Sel. Top. Appl. Earth Obs. Remote Sens.* **2013**, *6*, 942–952.
26. Wu, Y.; Zhang, S.; Kang, H.; Yeo, T.S. Fast marginalized sparse Bayesian learning for 3-D interferometric ISAR image formation via super-resolution ISAR imaging. *IEEE J. Sel. Top. Appl. Earth Obs. Remote Sens.* **2015**, *8*, 4942–4951.
27. Zhang, S.; Zhang, W.; Zong, Z.; Tian, Z.; Yeo, T.S. High-resolution bistatic ISAR imaging based on two-dimensional compressed sensing. *IEEE Trans. Antennas Propag.* **2015**, *63*, 2098–2111.

28. Tropp, J.A.; Gilbert, A.C. Signal recovery from random measurements via orthogonal matching pursuit. *IEEE Trans. Inf. Theory* **2007**, *53*, 4655–4666.
29. Chen, S.; Donoho, D.; Saunders, M.A. Atomic decomposition by basis pursuit. *SIAM J. Sci. Comput.* **1999**, *20*, 33–61.
30. Gorodnitsky, I.F.; Rao, B.D. Sparse signal reconstructions from limited data using focuss: A re-weighted minimum norm algorithm. *IEEE Trans. Signal Process.* **1997**, *45*, 699–716.
31. Candes, E.; Wakin, M.B.; Boyd, S.P. Enhancing sparsity by reweighted  $l_1$  minimization. *J. Fourier Anal. Appl.* **2008**, *14*, 877–905.
32. Fang, J.; Li, J.; Shen, Y.; Li, H.B.; Li, S. Super-resolution compressed sensing: An iterative reweighted algorithm for joint parameter learning and sparse signal recovery. *IEEE Signal Process. Lett.* **2014**, *21*, 761–765.
33. Shen, Y.; Fang, J.; Li, H.B. Exact reconstruction analysis of log-sum minimization for compressed sensing. *IEEE Signal Process. Lett.* **2013**, *20*, 1223–1226.
34. Rohling, H. Radar CFAR thresholding in clutter and multiple target situations. *IEEE Trans. Aerosp. Electron. Syst.* **1983**, *19*, 608–621.



© 2016 by the authors; licensee MDPI, Basel, Switzerland. This article is an open access article distributed under the terms and conditions of the Creative Commons Attribution (CC-BY) license (<http://creativecommons.org/licenses/by/4.0/>).